Partially Locked Low-Angle Normal Faults in Cohesive Upper Crust

X. P Yuan, J.-a. Olive, J. Braun

Tectonics

RESEARCH ARTICLE
10.1029/2019TC005753

Partially Locked Low-Angle Normal Faults in Cohesive Upper Crust

X. P. Yuan[1], J.-A. Olive[2], and J. Braun[1]

[1]Helmholtz Centre Potsdam, German Research Centre for Geosciences (GFZ), Potsdam, Germany, [2]Laboratoire de Géologie, Ecole Normale Supérieure/CNRS UMR 8538, PSL Research University, Paris, France

Key Points:
- We use Limit Analysis to investigate the feasibility of slip on partially active low-angle normal faults (LANFs) in cohesive upper crust
- Crustal cohesion enables slip on high-friction LANFs, and fault cohesion enables slip on partially active LANFs with steep splays
- Different locking depths on the Alto Tiberina (Italy) and western Corinth (Greece) LANFs reflect differences in fault cohesion

Supporting Information:
- Supporting Information S1

Correspondence to:
X. P. Yuan, Helmholtz Centre Potsdam, German Research Centre for Geosciences (GFZ), Potsdam, Germany
xyuan@gfz-potsdam.de

Citation:
Yuan, X., Olive, J.-A., & Braun, J. (2020). Partially locked low-angle normal faults in cohesive upper crust. *Tectonics*, *39*, e2019TC005753. https://doi.org/10.1029/2019TC005753

Received 10 JUL 2019
Accepted 7 FEB 2020
Accepted article online 10 FEB 2020

Abstract It is well established that slip on a frictionally weak low-angle normal fault (LANF) can be more favorable than breaking a steep fault in strong crust. Very few studies, however, have considered the specific effect of crust and fault cohesion on LANF viability. We do so using Limit Analysis, a methodology for predicting the optimal orientation of faults with varying strength subjected to a specific set of boundary conditions. Accounting for crustal cohesion in our models reduces the lowest admissible LANF dip and even allows slip on high-friction LANFs if the contrast between crust and fault cohesion is large. Fault cohesion, however, increases the lowest admissible LANF dip and introduces a locking depth above which LANF slip is not mechanically feasible. This is consistent with observations of steep splay faults rooting onto LANFs in a variety of settings. We further demonstrate that locking depth can help constrain LANF cohesion, friction, and fluid pressure on the Alto Tiberina (Italy) and western Corinth (Greece) LANFs. Specifically, assuming a measured fault friction of 0.2–0.3, we find that the shallow locking depth of the Alto Tiberina fault requires either (1) moderate fluid overpressure (57% of lithostatic) with cohesion of 8–12 MPa or (2) strong overpressure (77% of lithostatic) with cohesion of 13–20 MPa along the fault. By contrast, the larger locking depth characterizing the western Corinth LANF can reflect greater fault cohesion.

1. Introduction

Low-angle normal faults (LANFs) are highly localized brittle shear zones that dip below 30° and often accommodate large amounts of extension in the upper crust. LANFs have been extensively documented in the field and through seismic imaging in settings such as the Basin and Range province (Allmendinger et al., 1983; Niemi et al., 2004; Wernicke, 1981), the Iberia-Newfoundland margins (Manatschal et al., 2007; Ranero & Pérez-Gussinyé, 2010), and the Northern Apennines (Anderlini et al., 2016; Barchi et al., 1998; Chiaraluce et al., 2007; Collettini, 2011). Their widespread existence, however, challenges classical theories of brittle failure, which preclude the formation of normal faults dipping below 45° under Andersonian stress conditions, that is, horizontal and vertical principal stresses (Anderson, 1951).

It has therefore been proposed that LANFs may (1) form through flexural-isostatic rotation of initially steeper faults (Buck, 1988; Wernicke & Axen, 1988), (2) initiate at a shallow dip in a non-Andersonian stress field (e.g., Spencer & Chase, 1989), (3) result from the extensional reactivation of preexisting low-angle faults such as shallow-dipping thrusts (Collettini & Sibson, 2001; DeCelles & Coogan, 2006; Sibson, 1985; Yuan et al., 2018), or (4) invoke specific rheological properties of shear zones such as dilatancy (e.g., Lecomte et al., 2012) or complex feedbacks with underlying ductile deformation (Regenauer-Lieb et al., 2006). Models of the third category typically assess the mechanical conditions under which slipping on a shallow-dipping fault requires a lower differential stress than breaking a new steep fault in strong, intact crust (Choi & Buck, 2012; Forsyth, 1992; Sibson, 1985). In rocks characterized by Byerlee friction (~0.6) subjected to Andersonian stresses, slipping on preexisting planes shallower than 30° requires a tensile horizontal stress, which could be achieved through elevated fluid pressure. This, however, would favor hydrofracture over normal faulting, which would act to maintain fluid pressure near a hydrostatic state. Thus, 30° is referred to as a theoretical lockup angle below which fault reactivation is implausible (e.g., Collettini & Sibson, 2001). This lockup angle can be lowered to below 20° if LANF gouges contain very weak phyllosilicates (e.g., smectite, with friction coefficients <0.2), similar to those sampled on the San Andreas strike-slip fault at 2.7-km depth (e.g., Carpenter et al., 2011; Lockner et al., 2011). While weak clay minerals in fault gouges constitute an appealing solution to the

LANF paradox, they are not likely to be found beyond the uppermost few kilometers of the crust where temperatures exceed ~ 200 °C. Although weak phyllosilicates can be present along some faults at all depths within the entire seismogenic layer (e.g., Collettini et al., 2019), no weak phyllosilicates were sampled in the exhumed portions of some LANFs such as the Whipple detachment fault (Western United States), which primarily features quartz-rich ultracataclasites and chlorite-rich breccia with friction coefficients in excess of ~0.3 (Collettini & Sibson, 2001, and references therein). Invoking large contrasts in frictional strength between fault rocks and the surrounding crust may therefore not suffice to explain the mechanical viability of all LANFs.

While LANF friction has received significant attention, the effects of contrasting cohesion between normal faults and the surrounding crust remain to be fully elucidated. This is in part because many studies have relied on critical Coulomb wedge (CCW) theory to place quantitative constraints on LANF friction and fluid pressure. CCW theory (Hayman et al., 2003; Xiao et al., 1991; Yuan et al., 2018) reduces the LANF problem to the deformation of its hanging-wall wedge. By doing so, CCW theory yields the maximum fault friction (or minimum fluid pressure) that favors slip on a LANF (stable regime) as opposed to breaking steep faults in the hanging wall (i.e., internal deformation of the wedge in the subcritical regime). CCW theory is however limited to cohesionless materials, because introducing a stress scale would break down the self-similar nature of the problem. Yet crustal cohesion may have a strong effect on the stability of LANFs. On the one hand, breaking a new steep fault in cohesive upper crust requires more energy than in cohesionless rock. Under conditions that make breaking new steep faults more mechanically difficult, slipping on a weak preexisting LANF may therefore occur over a wider range of fault friction and fluid pressure. For example, Axen and Selverstone (1994) and Axen (2004) showed that slip on the Whipple detachment fault is possible with LANF friction of 0.6 if tensile strength and cohesion of the fault surroundings are taken into account, assuming that fluid pressure can be high in the bulk of the upper crust. On the other hand, if a preexisting LANF contains cohesive lithologies, and its strength contrast relative to the surrounding crust is reduced, LANF activity may become less favorable (Yuan et al., 2018).

Choi and Buck (2012) did consider the influence of cohesion in determining whether rotation of a detachment fault should result in the formation of new steep faults delineating the rider blocks commonly found above core complexes. Their study relied on differential stress estimates rather than CCW theory and pointed out that breaking steep faults may not be favorable below some characteristic depth. This pattern of steep faults rooting onto a LANF is found at several well-studied sites. For example, the Alto Tiberina fault (Northern Apennines, Italy, Figure 1a) extends all the way to the surface but features multiple steep splays above ~3 km. Further, geodetic studies have revealed that the uppermost portion of the LANF is locked (Anderlini et al., 2016; Chiaraluce et al., 2007; Hreinsdottir & Bennett, 2009), suggesting that shallow extension is accommodated by more mechanically favorable steep splays. A similar configuration can be inferred below the Western Gulf of Corinth (Greece, Figure 1b), where microseismicity illuminates a deep LANF below ~7 km (Chéry, 2001; Lambotte et al., 2014; Rigo et al., 1996). Steep, north-dipping faults such as the Aigion and Helike faults likely root onto the LANF at shallower crustal levels, where slip on the LANF may be mechanically unfavorable.

From a theoretical perspective, the existence of a characteristic depth below which LANFs can slip is readily explained by crust and fault cohesion imposing a characteristic stress and thus length scale to the system. This was recognized by Choi and Buck (2012). As their focus was on rider block development above shallow LANFs that steepen with depth, they did not consider planar LANFs with steep splays (Figures 1a and 1b). Our study generalizes their approach by assessing LANF stability from an energy perspective (e.g., Forsyth, 1992) rather than by considering the differential stresses acting on the fault. This is done through the Limit Analysis method (Yuan et al., 2015), which allows us to extend classical extensional CCW theory to cohesive materials. We further extend the results of Choi and Buck (2012) by proposing a methodology that constrains LANF strength from estimates of its locking depth.

2. Limit Analysis of Partially Active LANFs

We model LANFs using the kinematic approach of Limit Analysis. This semi-analytical method was described in detail by Salençon (1974, 2002) and Maillot and Leroy (2006) and is summarized in Supporting Information Text S1. Limit Analysis identifies the optimal geometry of a set of faults subjected to far-field loading (also referred to as an optimal "failure mechanism") with specified rheological properties. To do

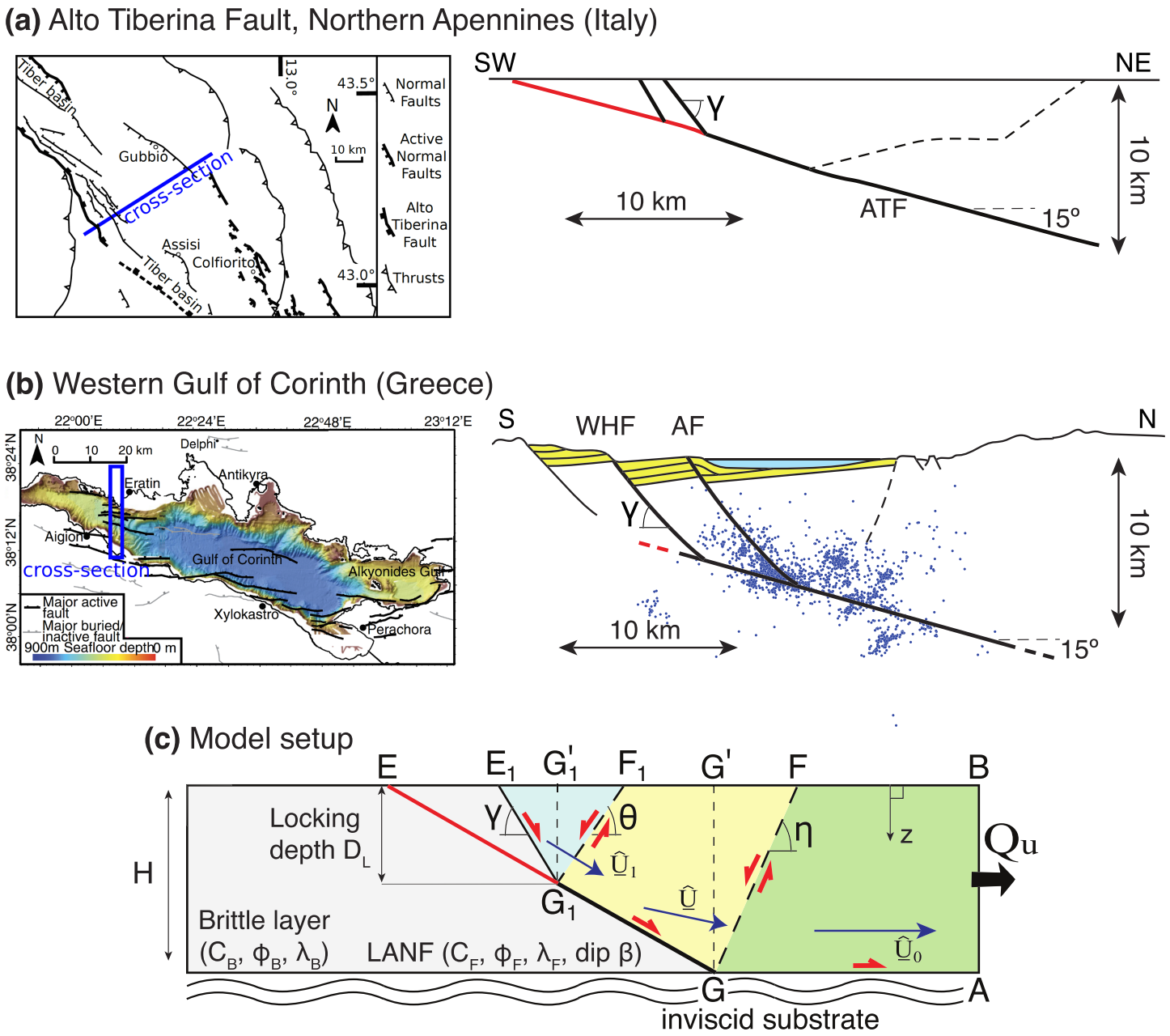

Figure 1. (a) Regional map (modified from Collettini & Barchi, 2002) and cross section through the Alto Tiberina fault, northern Apennines, Italy. Fault geometry (black lines) is interpreted from seismic profiles (Chiaraluce et al., 2007; Mirabella et al., 2011). Red segment corresponds to locked sections. (b) Regional map (Bell et al., 2018) and cross section through the western Gulf of Corinth, Greece, modified from Rigo et al. (1996) and Chéry (2001). Blue dots represent microseismicity illuminating a shallow-dipping fault plane (Lambotte et al., 2014). (c) Model setup for Limit Analysis of an extending brittle layer sitting above an inviscid substrate. Our model optimizes the failure mechanism of a partially active LANF (GG_1) in terms of the locking depth D_L, the dips of fault G_1E_1 and of axial surfaces GF, G_1F_1, which root onto the LANF. Note that this mechanism is valid for both fully active and fully locked LANFs, depending on the optimum value of locking depth D_L relative to the layer thickness H. $D_L = 0$ corresponds to a fully active LANF, and $D_L = H$ indicates a fully locked LANF.

so, one first defines a "virtual velocity field" describing the piecewise rigid displacement induced by slip on faults. One can then derive an upper bound for the far-field tectonic force Q_u that is necessary to activate a given fault geometry. This is done through the principle of virtual powers and with the constraint that the Mohr-Coulomb failure criterion must be met on all slipping faults. The fundamental postulate of Limit Analysis is that the optimal fault geometry is associated with the lowest upper bound on the boundary force (i.e., $Q_{lu} = \min\left(Q_u\right)$). This is due to the fact that when the boundary force is increased from zero to a high value (representing, e.g., the onset of regional tectonic stresses), the array of faults under consideration will

be activated when the boundary force reaches the minimum driving force. The optimal geometry is found by minimizing Q_u over all possible fault geometries (e.g., dips and depth extent). In contrast to numerical geodynamic modeling, the semi-analytical nature of Limit Analysis enables rapid exploration of a very wide parameter space. It is also noteworthy that under a simple Andersonian stress state, Limit Analysis is equivalent to integrating the differential stresses considered by Choi and Buck (2012) over the thickness of the upper crust, assuming a flat free surface and no basal shear stress. Here we apply this approach to identify the most favorable normal fault geometry for a wide range of rheological conditions, specifically crust and fault cohesion, friction, and fluid pressure.

Our model setup is presented in Figure 1c. The brittle upper crust, of thickness H and density $\rho = 2,700$ kg/m^3, is composed of a uniform Coulomb (frictional and cohesive) layer overlying the lower crust, which is treated as an inviscid substrate to generate much lower differential stresses than the upper crust (e.g., Buck, 1988; Choi et al., 2013; Forsyth, 1992). A homogeneous and planar LANF cuts through the brittle layer at a dip β. Fault cohesion C_F and friction angle φ_F are assumed lower than those of the intact layer bulk material C_B and φ_B, respectively. The crustal layer is saturated with aqueous fluids of density $\rho_f = 1,000$ kg/m^3 that exert a pore pressure p_f. Following Hubbert and Rubey (1959), we define fluid pressure ratio $\lambda = p_f/(\rho g z)$ such that hydrostatic and lithostatic fluid pressures correspond to $\lambda = \rho_f/\rho$ and $\lambda = 1$, respectively. g refers to the acceleration of gravity (9.81 m/s^2), and z is depth below the layer surface. The fluid pressure ratio in the brittle layer, λ_B, and along the LANF, λ_F, is assumed homogeneous. For simplicity, the value of λ_B is set to the hydrostatic value of 0.37, and μ_B is kept at 0.58 (friction angle $\varphi_B = 30°$) throughout the following analysis.

As the brittle layer gets strained on its lateral boundary (AB), it slips against the lower crust (AG) without resistance. Internal deformation of the upper crust occurs on a partially active LANF between points G and G_1 (Figure 1c). Because no slip occurs on segment (EG_1) of the LANF, we refer to the depth of point G_1 as the locking depth D_L. An axial surface GF, dipping at an angle η, separates rigid block $ABFG$ (green in Figure 1c) above the inviscid substrate and block FGG_1F_1 (yellow) above the LANF. While axial surfaces may correspond to actual faults, they are primarily introduced to separate rigid hanging-wall blocks and thus simplify the description of distributed (e.g., flexural) deformation when performing Limit Analysis. Slip on fault (GG_1) is connected above depth D_L to a steep normal fault (E_1G_1) of dip γ and its axial surface of dip θ. It is noteworthy that this generic mechanism accounts for a full spectrum of geometries between (and including) fully active and fully locked LANFs, depending on the length (L_{GG_1}) of the active LANF. We construct the virtual velocity field ($\underline{\hat{U}}$, $\underline{\hat{U}}_0$, $\underline{\hat{U}}_1$, $\underline{\hat{J}}$, $\underline{\hat{J}}_1$) for each failure mechanism (Text S2) to obtain the upper-bound force Q_u assuming mechanical equilibrium. This velocity field does not need to be the exact velocity field and is thus referred to as virtual. It corresponds to a simplified case used to obtain an analytical solution for Q_u (Cubas et al., 2008; Maillot & Leroy, 2006; Pons & Leroy, 2012; Yuan et al., 2015).

To facilitate our calculations, we nondimensionalize our parameters in the following way: Distances L_{XY} (from point X to point Y) are normalized by layer thickness H, and areas S_{XYZ} (with apexes X, Y, and Z) are normalized by H^2. Crust and fault cohesions (C_B, C_F) are normalized by the reference lithostatic stress $\rho g H$. As detailed in Text S3, the upper-bound force Q_u, normalized by $\rho g H^2$, can be expressed as

$$\begin{aligned}\tilde{Q}_u =& \tilde{C}_B \tilde{L}_{G_1E_1} \cos(\varphi_B)\hat{U}_1 + \tilde{C}_B \tilde{L}_{G_1F_1} \cos(\varphi_B)\hat{J}_1 + \tilde{C}_B \tilde{L}_{GF} \cos(\varphi_B)\hat{J} + \tilde{C}_F \tilde{L}_{GG_1} \cos(\varphi_F)\hat{U} \\ & - (1-\tilde{\rho}_f)\left[\tilde{S}_{E_1F_1G_1}\hat{U}_1 \sin(\gamma-\varphi_B) + \tilde{S}_{GG_1F_1F}\,\hat{U}\sin(\beta-\varphi_F)\right] \\ & - \left[(\lambda_B-\lambda_{hydro})\,\tilde{S}_{E_1G_1'G_1}\hat{U}_1\frac{\sin(\varphi_B)}{\cos(\gamma)} + (\lambda_B-\lambda_{hydro})\,\tilde{S}_{F_1G_1G_1'}\hat{J}_1\frac{\sin(\varphi_B)}{\cos(\theta)}\right. \\ & \left. +(\lambda_B-\lambda_{hydro})\,\tilde{S}_{GG'F}\hat{J}\,\frac{\sin(\varphi_B)}{\cos(\eta)} + (\lambda_F-\lambda_{hydro})\,\tilde{S}_{GG_1G_1'G'}\hat{U}\,\frac{\sin(\varphi_F)}{\cos(\beta)}\right],\end{aligned} \tag{1}$$

where dimensionless scalars are indicated by a tilde symbol. For a given set of fault properties (dip, cohesion, friction, and fluid pressure), we identify the optimal LANF and splay geometry by minimizing $\tilde{Q}_u$ over the whole family of failure mechanisms (i.e., variables of $\tilde{D}_L$, γ, θ, and η in Figure 1c). The minimization is carried out through a simple grid search algorithm, which is provided as FORTRAN routines in the Supporting Information. This enables us to assess whether, for a given combination of cohesion, friction, and fluid pressure, the most favorable fault geometry is a fully active LANF (i.e., with a dimensionless locking depth of $\tilde{D}_L = 0$), a partially active LANF with a steep splay ($0 < \tilde{D}_L < 1$), or a steep fault cutting through the entire upper crust (equivalent to a fully locked LANF, $\tilde{D}_L = 1$). In the following, we focus on mapping these various regimes (Figure 2).

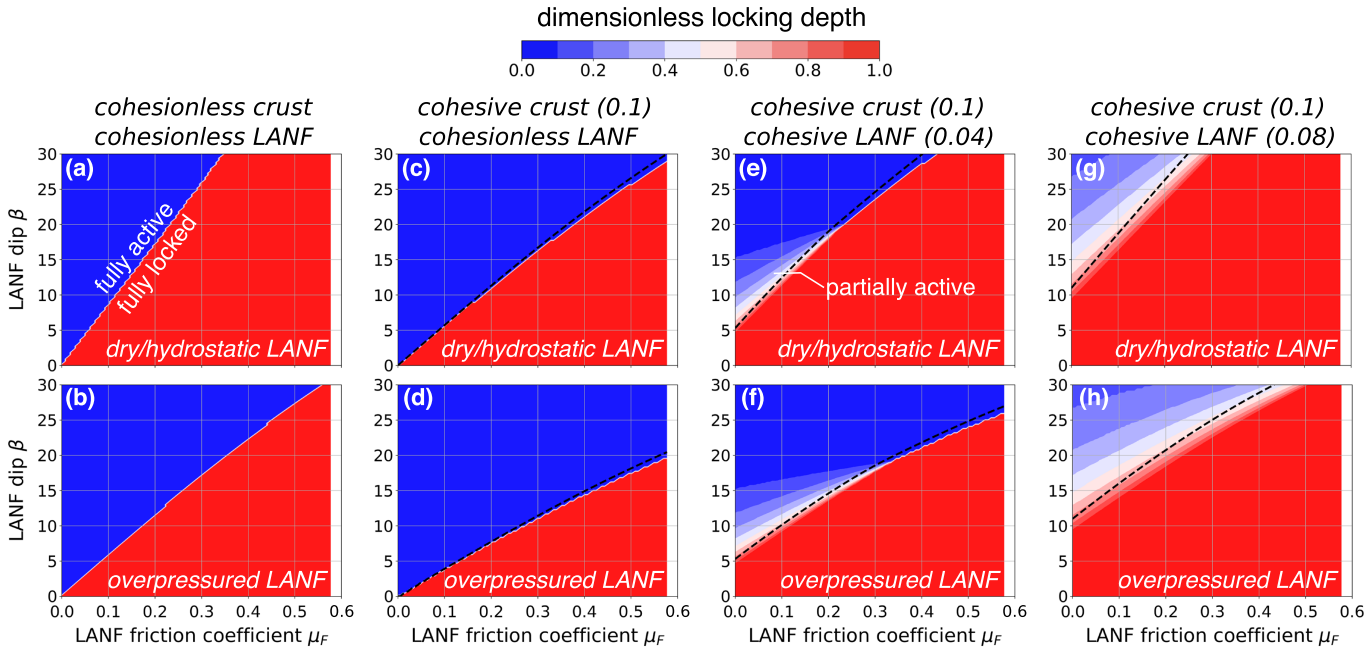

Figure 2. Dimensionless locking depth $\tilde{D}_L$ as a function of LANF dip β and friction coefficient $\mu_F = \tan(\varphi_F)$, assuming a dry/hydrostatic fault ($\lambda_F = \lambda_{hydro} = 0$ or 0.37, first row) versus an overpressured fault ($\lambda_F = \lambda_{hydro} + 0.2$, second row). (a, b) Cohesionless case: $\tilde{C}_B = \tilde{C}_F = 0$; (c, d) cohesive crust: $\tilde{C}_B = 0.1$, and cohesionless fault: $\tilde{C}_F = 0$; (e, f) cohesive crust: $\tilde{C}_B = 0.1$, and cohesive fault: $\tilde{C}_F = 0.04$; (g, h) cohesive crust: $\tilde{C}_B = 0.1$, and cohesive fault: $\tilde{C}_F = 0.08$. In (c)–(h), dashed line corresponds to $\tilde{Q}_{lu} = 0$ and thus marks the boundary between tensile and compressive boundary force.

3. Results

Figure 2 shows the effect of friction, cohesion, and fluid pressure on the admissible dips of a LANF. Codes and instructions to reproduce this figure are provided as part of the Supporting Information. In Figure 2, the blue domain marks the range of parameters for which the LANF can be fully active; that is, LANF cuts through the entire upper crust. In the red domain, however, slip on a steep fault (E_1G_1 in Figure 1c) dipping at $\pi/4 + \varphi_B/2$ and cutting through the entire upper crust requires less force than activating the LANF. The color scale in Figure 2 indicates intermediate cases where the LANF may be active below some locking depth $\tilde{D}_L$.

3.1. Cohesionless LANFs in Cohesionless Crust

In the case where both the LANF and the surrounding rocks are cohesionless (Figure 2a), dry/hydrostatic LANFs with $\mu_F = 0.2$ can be fully active (i.e., $\tilde{D}_L = 0$) with dips as low as 17.2°. If the fault experiences moderate fluid overpressures (e.g., $\lambda_F = 0.57$), this dip can be slightly lowered (e.g., 12°). In a more general sense, the critical dip β_c, below which cohesionless LANFs cannot be active, strongly depends on fault friction μ_F. This critical dip β_c can be obtained with CCW theory (Xiao et al., 1991; Yuan et al., 2015), which gives

$$\beta_c = \frac{1}{2}\arcsin\left[\frac{(1-\lambda_F)\sin(\varphi_F)}{(1-\lambda_B)\sin(\varphi_B)} - \frac{(\lambda_F-\lambda_B)\sin(\varphi_F)}{1-\lambda_B}\right] + \frac{1}{2}\varphi_F, \tag{2}$$

and exactly matches the boundary between fully active and fully locked LANFs predicted through Limit Analysis (Figures 2a and 2b). Equation (2) simply reflects a particular case of CCW theory with a flat surface ($\alpha = 0°$ in equation (B6) of Yuan et al., 2015) and vertical maximum principal stress (σ_1 is at $\Psi_O = 90°$ from the surface, see figure 2b of Xiao et al., 1991). It should be noted that $\varphi_F \geq 0$ in equation (2) follows a different sign convention compared to equation (B6) of Yuan et al. (2015). Our approach is thus equivalent to CCW theory in the cohesionless case, as the domain above the LANF can be regarded as a critical wedge. Unlike CCW theory, however, Limit Analysis is well suited for cases with crust and fault cohesion.

3.2. Cohesionless LANF in Cohesive Crust

Typical values of upper-crust cohesion are in the range of 10–50 MPa (Byerlee, 1978; Handin, 1966). We therefore focus on dimensionless cohesions $\tilde{C}_B \leq 0.1$, which corresponds to 27 and 40 MPa for $H = 10$ and 15 km, respectively. Figure 2c illustrates the case of a cohesionless fault in cohesive crust. Again, LANFs

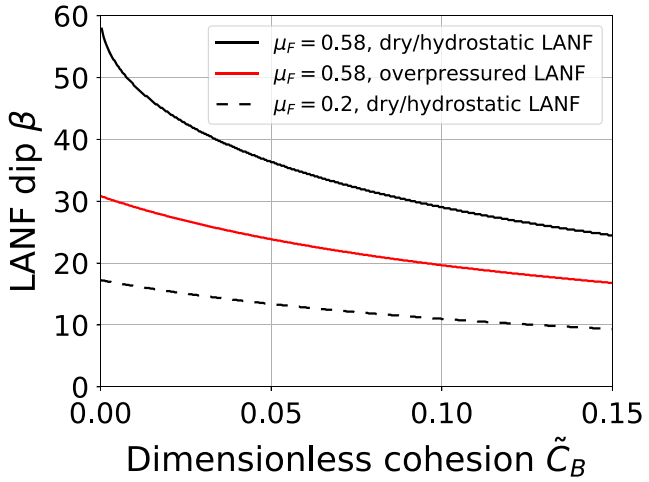

Figure 3. Lowest admissible LANF dip β as a function of dimensionless layer cohesion $\tilde{C}_B$ for a cohesionless fault of specified friction ($\mu_F = 0.2$) and fluid pressure ratio. The overpressured case corresponds to $\lambda_F = \lambda_{hydro} + 0.2 = 0.57$.

can only be active above a certain critical dip, which is ~40% lower than in the fully cohesionless case under the same fluid pressure conditions (Figure 2a vs. Figure 2c). For example, slip on an 11°-dipping hydrostatic cohesionless LANF with $\mu_F = 0.2$ is possible for $\tilde{C}_B = 0.1$, while such a fault would be fully locked in a cohesionless layer (see dashed curve in Figure 3). Increasing crust cohesion decreases the critical dip of cohesionless LANFs (Figure 4a). For example, the lowest admissible dip of a LANF with $\mu_F = 0.2$ decreases from 17.2° to 10.5° when crust cohesion $\tilde{C}_B$ is increased from 0 to 0.1, as shown in Figures 3 (dashed curve) and 4a. Figure 4a also shows that cohesionless LANFs can only be either fully active or fully locked. This reflects the fact that configurations minimizing $\tilde{Q}_u$ in equation (1) will only allow $\tilde{D}_L = 0$ or 1. Finally, we note that fluid overpressure also decreases the critical dip of LANFs in cohesive crust, over a wide range of LANF friction coefficients (e.g., increasing λ_F by 0.2 decreases the critical dip by ~30%, Figure 2c vs. Figure 2d).

3.3. Cohesive LANF in Cohesive Crust

Increasing fault cohesion $\tilde{C}_F$ while keeping crust cohesion constant (e.g., $\tilde{C}_B = 0.1$) leads to an increase in critical LANF dip (Figure 2c vs. Figure 2e), as it reduces the strength contrast between the fault and its host rock. Unlike cohesionless LANFs, however, cohesive LANFs may be partially active. This is, for example, the case under dry/hydrostatic conditions for cohesive LANFs with $\tilde{C}_F = 0.04$ and a friction coefficient lower than 0.23 ($0 < \tilde{D}_L < 1$, Figure 2e). Steeper LANFs are associated with shallower locking depths. However, low values of fault cohesion do not allow partially active LANFs and as such resemble the cohesionless LANF case. This is, for example, the case of LANFs with $\tilde{C}_F < 0.02$ and a friction coefficient of 0.2, assuming a crust cohesion of $\tilde{C}_B = 0.1$ (Figure 4b). Increasing fault cohesion to 0.04–0.08 introduces a nonzero locking depth. This depth increases with increasing fault cohesion on a LANF of constant dip. Finally, the stability domain of partially active LANFs can be extended by increasing fault cohesion (Figures 2g and 2h). It should be noted, however, that slip on LANFs that have dips close to their shallowest admissible dip requires a horizontal force $\tilde{Q}_u$ that is close to zero. The horizontal stress in the crust thus becomes close to net tensile, which would favor vertical hydrofracture over frictional slip. This limit is indicated as a dashed curve in Figures 2c–2h and represents a likely bound on LANF rheological properties (see section 4.1).

4. Implications for LANF Stability

4.1. Locking Depth as a Constraint on LANF Strength: Applications to the Alto Tiberina (Italy) and Western Corinth (Greece) LANFs

Accounting for crust and fault cohesion in our mechanical analysis of LANFs enables us to put stringent constraints on the rheologies of these systems. To demonstrate this, we apply our model to two active, 15°-dipping normal faults which connect with overlying, steep-dipping splay faults at different depths. The NE-dipping Alto Tiberina fault in the northern Apennines of Italy (Figure 1a) displaces the compressional structures of the Apenninic thrust belt with a few steep synthetic splays (Chiaraluce et al., 2007; Collettini & Barchi, 2002; Mirabella et al., 2011). The region comprises a cover sequence of sedimentary rocks deposited upon a Paleozoic metamorphic basement (Chiaraluce et al., 2007; Collettini & Barchi, 2002). The rock units at the base of the cover succession consist of late Triassic Evaporites overlain by Liassic platform carbonates, Jurassic-Oligocene pelagic sediments, and Miocene-Pliocene turbidites, as revealed by drilling and reflection seismic studies (Chiaraluce et al., 2007). The Alto Tiberina fault is known from geodetic studies (Anderlini et al., 2016; Hreinsdottir & Bennett, 2009) to be locked down to a depth of 4 ± 1 km. The depth extent of microseismicity in the region provides an estimate of the brittle layer thickness of $H = 14 \pm 2$ km (Chiaraluce et al., 2007). This yields a dimensionless locking depth of $\tilde{D}_L = 0.2$–0.4.

The Gulf of Corinth (Greece) is to first order an E-W striking half-graben structure accommodating N-S extension (Figure 1b), dominated by a series of N-dipping normal faults along its southern margin (e.g., Armijo et al., 1996; Bell et al., 2008, 2018). In the western Gulf of Corinth, steep normal faults such as the Western Helike and Aigion faults appear to root on a seismically active, shallow-dipping plane at a depth of 8 ± 1 km (Chéry, 2001; Lambotte et al., 2014; Rigo et al., 1996) (Figure 1b). Microseismicity on this plane

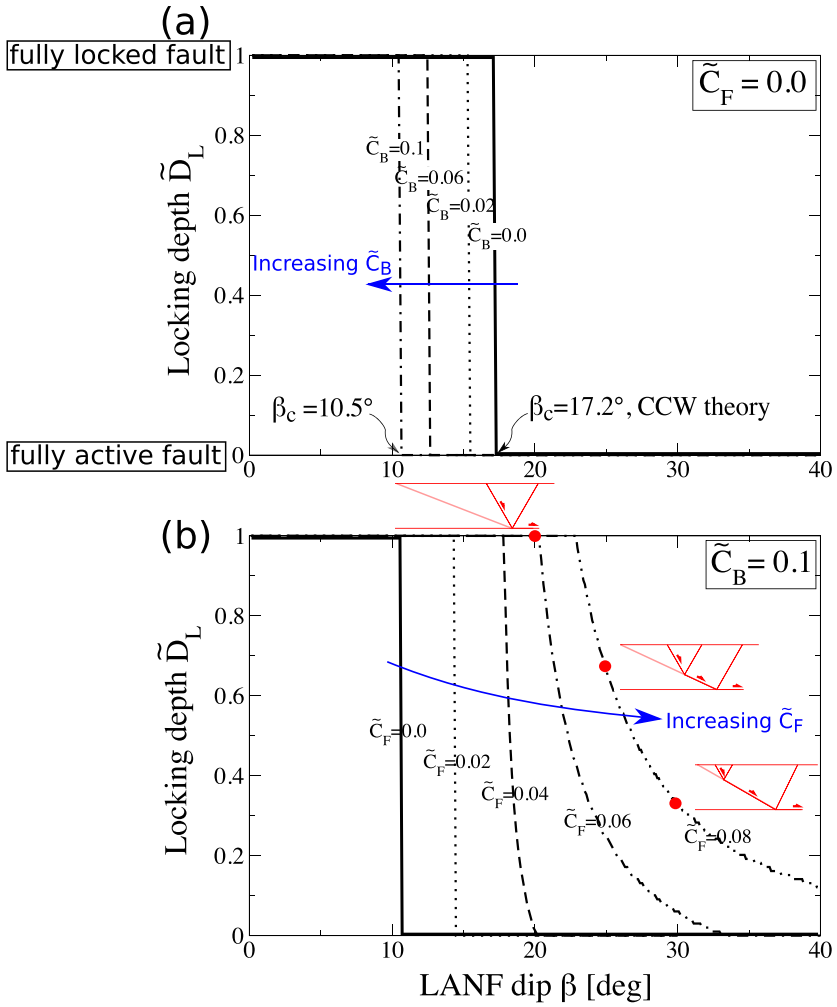

Figure 4. Dimensionless locking depth $\tilde{D}_L$ of LANF as a function of its dip β, assuming fault friction $\mu_F = 0.2$ ($\varphi_F = 11.3°$) and a dry/hydrostatic fault $\lambda_F = \lambda_{hydro} = 0$ or 0.37. (a) Crust cohesion $\tilde{C}_B$ varies between 0 and 0.1, and fault cohesion $\tilde{C}_F$ is set to 0. (b) Fault cohesion $\tilde{C}_F$ varies between 0 and 0.08, and $\tilde{C}_B$ is set to 0.1. In (a), Limit Analysis captures well the critical dip obtained with CCW theory for cohesionless crust and fault. Red cartoons in (b) show failure modes corresponding to $\beta = 20°$, 25°, and 30° for the case of $\tilde{C}_F = 0.08$. Fault dip $\beta = 20°$ corresponds to a fully locked LANF ($\tilde{D}_L = 1$). A partially active LANF is observed at $\beta = 25°$, and the locking depth reduces when fault dip is increased to 30°.

does not extend south of the steep-dipping faults. This suggests that the LANF is either absent or locked in this region. Few earthquakes occur beneath a depth of 12 ± 1 km (Lambotte et al., 2014); we therefore estimate a dimensionless locking depth of $\tilde{D}_L = 0.5$–0.9 in this system.

With a constraint on the value of $\tilde{D}_L$, we can now identify combinations of LANF cohesion and friction that make the observed geometries mechanically favorable. These are plotted in Figure 5 (codes and instructions to reproduce this figure are given in Text S4), under different assumptions regarding crust cohesion C_B and fault fluid pressure ratio λ_F. In Figure 5a, the dimensionless crust cohesion $\tilde{C}_B$ is assumed to be 0.05, which translates to 13–20 MPa for a brittle layer of thickness 10–15 km. In this case, LANF friction cannot exceed 0.17, and its cohesion must exceed 4–6 MPa ($\tilde{C}_F = 0.015$, 30% of $\tilde{C}_B$). A lower value of LANF friction is of course possible but requires a higher value of LANF cohesion to keep $\tilde{D}_L$ constant. In a more cohesive crust (e.g., 27–40 MPa, $\tilde{C}_B = 0.1$, Figure 5b), greater LANF cohesion is required to produce the observed values of $\tilde{D}_L$ over the same range of fault friction. In this configuration, however, the optimal tectonic force (the least upper-bound force $\tilde{Q}_{lu}$) necessary to drive slip on the partially active LANF may become positive if fault cohesion and friction exceed a limit indicated by a dashed line in Figures 5b and 5c. Since a net tensile horizontal stress, which would enable hydrofractures, is unlikely to prevail throughout the upper

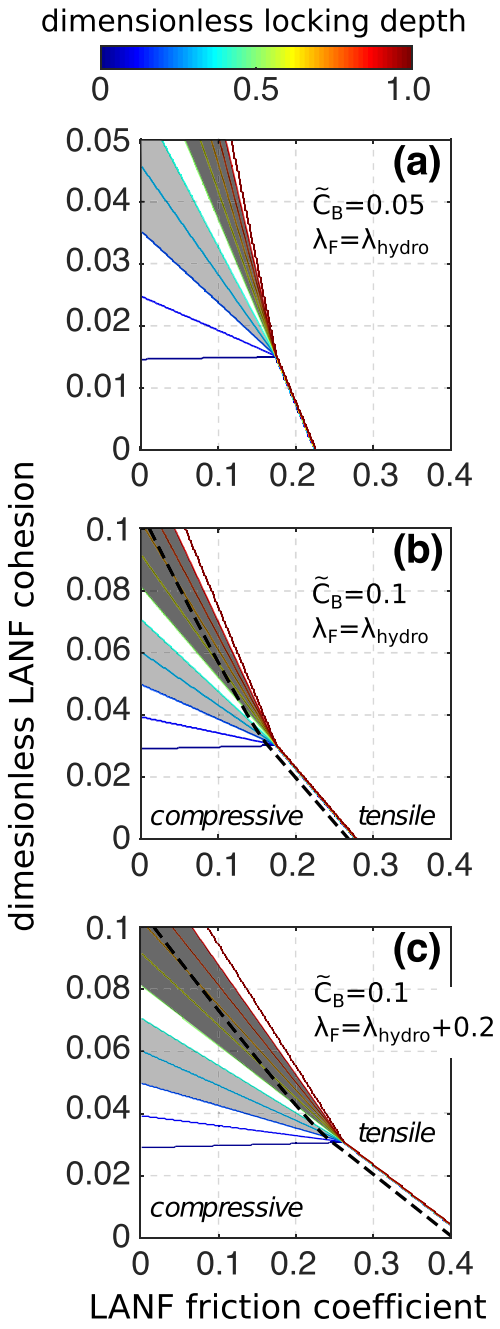

Figure 5. Combinations of cohesion $\tilde{C}_F$ and fault friction μ_F enabling slip on a partially active LANF of dip 15° and locking depth $\tilde{D}_L$ (color code), under various conditions: (a) $\tilde{C}_B = 0.05$ and hydrostatic fault; (b) $\tilde{C}_B = 0.1$ and hydrostatic fault; and (c) $\tilde{C}_B = 0.1$ and overpressured fault ($\lambda_F = \lambda_{hydro} + 0.2$). Dashed black line corresponds to $\tilde{Q}_{lu} = 0$ and thus marks the boundary between tensile and compressive boundary force. The gray-shaded areas correspond to locking depths observed on the Alto Tiberina ($\tilde{D}_L$ = 0.2–0.4, light gray shading) and western Corinth ($\tilde{D}_L$ = 0.5–0.9, dark gray shading) LANFs, see Figures 1a and 1b, respectively.

crust, the $\tilde{Q}_{lu} = 0$ contour can be considered a plausible upper bound on fault properties. Transitioning to a tensile $\tilde{Q}_{lu}$ is further facilitated if fluid overpressure occurs within the LANF (Figure 5c). Fluid overpressures ($\lambda_F = \lambda_{hydro} + 0.2$, Figure 5c) otherwise make larger values of LANF friction (as high as 0.25) plausible, for fault cohesion at 30% of $\tilde{C}_B$.

The lower value of $\tilde{D}_L = 0.2$–0.4 in the Alto Tiberina fault further imposes the conditions that both cohesion and friction be lower in this fault compared to the western Corinth LANF, as long as $\tilde{C}_B$ and λ_F remain comparable in both systems. Several studies have investigated the frictional properties of fault rocks from the Apennines (Collettini, Niemeijer, et al., 2009; Smith & Faulkner, 2010; Tesei et al., 2012). The weakest friction coefficients are typically measured in phyllosilicate-bearing gouge and range between 0.2 and 0.3 (Tesei et al., 2012). If these values measured near the surface are representative of friction in the deeper Alto Tiberina fault, then only a narrow subset of parameters allows slip on such a partially active system. If crust cohesion is in the range of 27–40 MPa, $\tilde{D}_L = 0.2 - 0.4$ requires either (1) a moderate fluid overpressure in the fault (e.g., $\lambda_F = 0.57$, Figure 5c) and a fault cohesion of 8–12 MPa (30% of layer cohesion) or (2) a large fluid overpressure (e.g., $\lambda_F = 0.77$, Figure S2b) and a fault cohesion of 17–20 MPa (50% of crust cohesion). Either way, fluid overpressure is required in the fault, which is consistent with borehole measurements indicating highly overpressured CO_2 beneath the Alto Tiberina fault breakaway (Chiodini et al., 2004).

Measurements of fault friction and fluid pressure are much less accessible for the deep-seated LANF of the western Gulf of Corinth. Lecomte et al. (2012) put forward the idea that this LANF should not be thought of as a plane but rather as a finite thickness zone where plastic compaction takes place in response to shear. The effect of compaction is to enable slip on shallow-dipping (20°) surfaces even with moderate-to-high friction coefficients (0.3–0.4). Our model instead focuses on the effect of cohesion while ignoring dilatancy. In particular, it predicts that if friction in the western Corinth LANF is similar to that of the Alto Tiberina fault (e.g., because similar phyllosilicate lithologies exist in their gouges), then greater cohesion in the Corinth LANF would suffice to explain the larger locking depth observed there (Figure 5). This is consistent with the work of Lambotte et al. (2014) and Bell et al. (2018) who concluded that the western Corinth LANF is likely an incipient (or recently reactivated) structure, in contrast to the more mature Alto Tiberina fault. A recently formed or reactivated fault may indeed not have experienced as much cohesion loss with accumulated strain as a mature fault.

Our model is broadly applicable to LANFs that formed through the reactivation of preexisting shallow-dipping structures (e.g., thrusts or other weak zones). We have specifically shown that if the preexisting structure has retained some cohesion, forming a partially active structure with steep splays can in some instances be more energetically favorable than reactivating the entire LANF all the way to the surface. The greater the LANF cohesion, the deeper the locking depth.

4.2. To What Extent Is Low Friction Necessary for LANF Slip?

Accounting for crust and fault cohesion brings new perspectives into the debate on whether LANF slip requires low fault friction (<0.3). For example, Collettini (2011) reviewed the fault rocks of nine LANFs, and several do not have evidence for frictionally weak minerals being present in

the deeper part of the upper crust or the seismogenic zone. We here look at cohesionless LANFs in cohesive crust and consider a dry/hydrostatic, high-friction LANF (e.g., $\mu_F = \mu_B = 0.58$, solid black curve in Figure 3). In a cohesionless crust (i.e., $\tilde{C}_B = \tilde{C}_F = 0$), the lowest admissible LANF dip is 60°, consistent with Andersonian-Byerlee faulting theory. Increasing crust cohesion however substantially reduces this critical dip (Figure 3). In particular, we find that high-friction LANFs can also be active with dips as low as 29° when fault cohesion is significantly lower than crust cohesion (e.g., $\tilde{C}_B = 0.1, \tilde{C}_F = 0$, Figures 2c and 3). This challenges the notion that LANFs necessarily involve low-friction materials (i.e., $\mu_F \ll 0.6$). Under dry/hydrostatic conditions, the lowest admissible dip of a cohesionless LANF can be reduced to 24° (Figure 3) in a cohesive crust with $\tilde{C}_B = 0.15$ (i.e., $C_B = 40$ and 60 MPa for a brittle layer thickness $H = 10$ and 15 km, respectively). It can be further reduced to 17° (red curve in Figure 3) if the fault is subject to moderate fluid overpressure ($\lambda_F = \lambda_{hydro} + 0.2$). Our results from the previous section however indicate that slip on cohesive LANFs, which can be partially active, does require a low-friction fault (<0.3).

4.3. Model Limitations

The premise of Limit Analysis is that the most favorable fault geometry would be associated with the least upper bound on the magnitude of the external driving force. In the particular cohesionless case, the good match between our Limit Analysis and the exact CCW theory (Yuan et al., 2015) constitutes a benchmark of our method. In nature, however, the external driving force may not adjust to reach and remain at a minimum corresponding to a certain fault geometry. Tectonic driving forces would be prescribed by the larger-scale geodynamics of the region, independently of a forming fault's geometry, and can even change over time. Nonetheless, many tectonic systems appear to evolve in a manner consistent with minimizing the amount of external work prescribed to the system (e.g., Cooke & Madden, 2014, and reference therein). Limit Analysis can be viewed as a subset of the more general work minimization framework (Cooke & Madden, 2014; McBeck et al., 2017), in that a given (evolving) tectonic load will at any time activate the optimally oriented fault array.

In our mechanical analysis, we assume homogeneous crust and fault properties that do not vary with depth for the sake of simplicity. We particularly assume a constant fluid pressure gradient at all depths. However, disequilibrium-compaction fluid pressures, which are widespread in sedimentary basins, lead to hydrostatic fluid pressure at shallow depths of a few kilometers above a fluid-retention depth, below which borehole data suggest that pore fluids become overpressured (e.g., Suppe, 2014). If a fault retains constant cohesion and friction with depth, then the change of fluid pressure gradient is also likely to control the LANF locking depth. More generally, the mechanisms investigated in this work on crust and fault cohesion may act along with material anisotropy and inhomogeneous fluid pressure gradient to control the optimal geometry of partially active LANFs.

The last important simplifying assumption in our model is that of an inviscid lower crust. This condition is likely to be met in high heat-flow extensional settings with a low viscosity lower crust (Buck, 1988), which does not impart strong shear stresses across the brittle-ductile transition (Nagel & Buck, 2006). It could also be justified by the existence of an evaporite layer that undergoes rapid creep and exerts minimal resistance to horizontal motions in the brittle domain. While beyond the scope of this contribution, the Limit Analysis framework is flexible enough to incorporate complications such as non-Andersonian stress fields, the existence of basal shear stress, or a topographic slope.

5. Conclusions

We have used Limit Analysis to identify energetically favorable LANF geometries, accounting for the effect of crust and fault friction, fluid pressure, and, for the first time, cohesion. Our main findings can be summarized as follows:

- Limit Analysis perfectly matches CCW theory when both crust and LANF are assumed cohesionless. In this case, LANFs are either fully active or fully locked.
- Increasing crustal cohesion reduces the lowest possible dip of a cohesionless LANF, which is again either fully active or fully locked.
- Limit Analysis also shows that even if a LANF is not frictionally weak compared to the surrounding crust (e.g., $\mu_F = \mu_B$), a fully active high-friction LANF can also be favorable if fault cohesion is much weaker than crust cohesion.

- Increasing fault cohesion increases the lowest possible dip of a LANF and introduces the possibility of partially active LANFs if fault cohesion exceeds ~30% of crust cohesion. Such partially active structures are analogous to geometries found at several well-studied LANFs.
- We apply our model to two partially active LANFs (the Alto Tiberina fault in Italy and the western Corinth LANF in Greece) to constrain LANF cohesion and friction. Assuming a reasonable crustal cohesion of 27–40 MPa, $\tilde{D}_L = 0.2$–0.4 in the Alto Tiberina fault requires either (1) moderate fluid overpressure in the fault (e.g., 57% of lithostatic pressure) with fault cohesion of about 8–12 MPa or (2) large fluid overpressure in the fault (e.g., 77% of lithostatic pressure) with fault cohesion of about 13–20 MPa. A more cohesive Corinth LANF, consistent with a more recent onset, would suffice to explain the greater locking depth observed there.

Acknowledgments
We thank Yves Leroy for helpful comments and Gary Axen for his feedback on an early draft. We also thank Cristiano Collettini and two anonymous reviewers for their helpful reviews. J.-A. O. was funded under NSF Project EAR-1650166 and benefited from an ENS "Actions Incitatives" grant. The codes to reproduce Figures 2 and 5 are available online (https://doi.org/10.5281/zenodo.3656853).

References

Allmendinger, R. W., Sharp, J. W., Von Tish, D., Serpa, L., Brown, L., Kaufman, S., et al. (1983). Cenozoic and Mesozoic structure of the eastern Basin and Range province, Utah, from COCORP seismic-reflection data. *Geology*, *11*(9), 532–536.

Anderlini, L., Serpelloni, E., & Belardinelli, M. E. (2016). Creep and locking of a low-angle normal fault: Insights from the Altotiberina fault in the Northern Apennines (Italy). *Geophysical Research Letters*, *43*, 4321–4329. https://doi.org/10.1002/2016GL068604

Anderson, E. M. (1951). *The dynamics of faulting*. London: Edinburgh.

Armijo, R., Meyer, B., King, G., Rigo, A., & Papanastassiou, D. (1996). Quaternary evolution of the Corinth Rift and its implications for the Late Cenozoic evolution of the Aegean. *Geophysical Journal International*, *126*(1), 11–53.

Axen, G. J. (2004). *Mechanics of low-angle normal faults* (pp. 46–91). New York: Columbia University Press.

Axen, G. J., & Selverstone, J. (1994). Stress state and fluid-pressure level along the Whipple detachment fault, California. *Geology*, *22*(9), 835–838.

Barchi, M. R., Minelli, G., & Pialli, G. (1998). The CROP 03 profile: A synthesis of results on deep structures of the Northern Apennines. *Memorie della Società Geologica Italiana*, *52*, 383–400.

Bell, R. E., Duclaux, G., Nixon, C. W., Gawthorpe, R. L., & McNeill, L. C. (2018). High-angle, not low-angle, normal faults dominate early rift extension in the Corinth Rift, central Greece. *Geology*, *46*(2), 115–118.

Bell, R. E., McNeill, L. C., Bull, J. M., & Henstock, T. J. (2008). Evolution of the offshore western Gulf of Corinth. *Geological Society of America Bulletin*, *120*(1-2), 156–178.

Buck, W. R. (1988). Flexural rotation of normal faults. *Tectonics*, *7*(5), 959–973.

Byerlee, J. (1978). Friction of rocks. *Pure and Applied Geophysics*, *116*(4-5), 615–626.

Carpenter, B., Marone, C., & Saffer, D. (2011). Weakness of the San Andreas Fault revealed by samples from the active fault zone. *Nature Geoscience*, *4*(4), 251–254.

Chéry, J. (2001). Core complex mechanics: From the Gulf of Corinth to the Snake Range. *Geology*, *29*(5), 439–442.

Chiaraluce, L., Chiarabba, C., Collettini, C., Piccinini, D., & Cocco, M. (2007). Architecture and mechanics of an active low-angle normal fault: Alto Tiberina Fault, northern Apennines, Italy. *Journal of Geophysical Research*, *112*, B10310. https://doi.org/10.1029/2007JB005015

Chiodini, G., Cardellini, C., Amato, A., Boschi, E., Caliro, S., Frondini, F., & Ventura, G. (2004). Carbon dioxide earth degassing and seismogenesis in central and southern Italy. *Geophysical Research Letters*, *31*, L07615. https://doi.org/10.1029/2004GL019480

Choi, E., & Buck, W. R. (2012). Constraints on the strength of faults from the geometry of rider blocks in continental and oceanic core complexes. *Journal of Geophysical Research*, *117*, B04410. https://doi.org/10.1029/2011JB008741

Choi, E., Buck, W. R., Lavier, L. L., & Petersen, K. D. (2013). Using core complex geometry to constrain fault strength. *Geophysical Research Letters*, *40*, 3863–3867. https://doi.org/10.1002/grl.50732

Collettini, C. (2011). The mechanical paradox of low-angle normal faults: Current understanding and open questions. *Tectonophysics*, *510*(3-4), 253–268.

Collettini, C., & Barchi, M. R. (2002). A low-angle normal fault in the Umbria region (Central Italy): A mechanical model for the related microseismicity. *Tectonophysics*, *359*(1-2), 97–115.

Collettini, C., Niemeijer, A., Viti, C., & Marone, C. (2009). Fault zone fabric and fault weakness. *Nature*, *462*(7275), 907–910.

Collettini, C., & Sibson, R. H. (2001). Normal faults, normal friction? *Geology*, *29*(10), 927–930.

Collettini, C., Tesei, T., Scuderi, M. M., Carpenter, B. M., & Viti, C. (2019). Beyond Byerlee friction, weak faults and implications for slip behavior. *Earth and Planetary Science Letters*, *519*, 245–263.

Cooke, M. L., & Madden, E. H. (2014). Is the Earth lazy? A review of work minimization in fault evolution. *Journal of Structural Geology*, *66*, 334–346.

Cubas, N., Leroy, Y. M., & Maillot, B. (2008). Prediction of thrusting sequences in accretionary wedges. *Journal of Geophysical Research*, *113*, 1–21. https://doi.org/10.1029/2008JB005717

DeCelles, P. G., & Coogan, J. C. (2006). Regional structure and kinematic history of the Sevier fold-and-thrust belt, central Utah. *Geological Society of America Bulletin*, *118*(7-8), 841–864.

Forsyth, D. W. (1992). Finite extension and low-angle normal faulting. *Geology*, *20*(1), 27–30.

Handin, J. (1966). *Section 10: Strength and ductility*: Geological Society of America Memoirs.

Hayman, N. W., Knott, J. R., Cowan, D. S., Nemser, E., & Sarnawojcicki, A. M. (2003). Quaternary low-angle slip on detachment faults in Death Valley, California. *Geology*, *31*(4), 343–346.

Hreinsdottir, S., & Bennett, R. A. (2009). Active aseismic creep on the Alto Tiberina low-angle normal fault, Italy. *Geology*, *37*(8), 683–686.

Hubbert, M. K., & Rubey, W. W. (1959). Role of fluid pressure in mechanics of overthrust faulting: I. Mechanics of fluid-filled solids and its application to overthrust faulting. *Geological Society of America Bulletin*, *70*, 115–166.

Lambotte, S., Lyon-Caen, H., Bernard, P., Deschamps, A., Patau, G., Nercessian, A., et al. (2014). Reassessment of the rifting process in the western Corinth Rift from relocated seismicity. *Geophysical Journal International*, *197*(3), 1822–1844.

Lecomte, E., Pourhiet, L. L., & Lacombe, O. (2012). Mechanical basis for slip along low-angle normal faults. *Geophysical Research Letters*, *39*, 75–81. https://doi.org/10.1029/2011GL050756

Lockner, D. A., Morrow, C., Moore, D., & Hickman, S. (2011). Low strength of deep San Andreas fault gouge from SAFOD core. *Nature*, *472*(7341), 82–85.

Maillot, B., & Leroy, Y. M. (2006). Kink-fold onset and development based on the maximum strength theorem. *Journal of the Mechanics and Physics of Solids*, *54*(10), 2030–2059.

Manatschal, G., Müntener, O., Lavier, L., Minshull, T., & Péron-Pinvidic, G. (2007). Observations from the Alpine Tethys and Iberia–Newfoundland margins pertinent to the interpretation of continental breakup. *Geological Society, London Special Publications*, *282*(1), 291–324.

McBeck, J. A., Cooke, M. L., Herbert, J. W., Maillot, B., & Souloumiac, P. (2017). Work optimization predicts accretionary faulting: An integration of physical and numerical experiments. *Journal of Geophysical Research: Solid Earth*, *122*, 7485–7505. https://doi.org/10.1002/2017JB013931

Mirabella, F., Brozzetti, F., Lupattelli, A., & Barchi, M. (2011). Tectonic evolution of a low-angle extensional fault system from restored cross-sections in the Northern Apennines (Italy). *Tectonics*, *30*, TC6002. https://doi.org/10.1029/2011TC002890

Nagel, T., & Buck, W. R. (2006). Channel flow and the development of parallel-dipping normal faults. *Journal of Geophysical Research*, *111*, B08407. https://doi.org/10.1029/2005JB004000

Niemi, N. A., Wernicke, B. P., Friedrich, A. M., Simons, M., Bennett, R. A., & Davis, J. L. (2004). BARGEN continuous GPS data across the eastern Basin and Range province, and implications for fault system dynamics. *Geophysical Journal International*, *159*(3), 842–862.

Pons, A., & Leroy, Y. M. (2012). Stability of accretionary wedges based on the maximum strength theorem for fluid-saturated porous media. *Journal of the Mechanics and Physics of Solids*, *60*, 643–664.

Ranero, C. R., & Pérez-Gussinyé, M. (2010). Sequential faulting explains the asymmetry and extension discrepancy of conjugate margins. *Nature*, *468*(7321), 294–9.

Regenauer-Lieb, K., Weinberg, R. F., & Rosenbaum, G. (2006). The effect of energy feedbacks on continental strength. *Nature*, *442*(7098), 67–70.

Rigo, A., LyonCaen, H., Armijo, R., Deschamps, A., Hatzfeld, D., Makropoulos, K., et al. (1996). A microseismic study in the western part of the Gulf of Corinth (Greece): Implications for large-scale normal faulting mechanisms. *Geophysical Journal International*, *126*(3), 663–688.

Salençon, J. (1974). *Théorie de la plasticité pour les applications à la mécanique des sols*. Paris: Eyrolles.

Salençon, J. (2002). *De l'élasto-plasticité au calcul à la rupture, École Polytechnique*. Paris: Palaiseau, and Ellipses.

Sibson, R. H. (1985). A note on fault reactivation. *Journal of Structural Geology*, *7*(6), 751–754.

Smith, S. A. F., & Faulkner, D. R. (2010). Laboratory measurements of the frictional properties of the Zuccale low-angle normal fault, Elba Island, Italy. *Journal of Geophysical Research*, *115*, 1448–1470. https://doi.org/10.1029/2008JB006274

Spencer, J. E., & Chase, C. G. (1989). Role of crustal flexure in initiation of low-angle normal faults and implications for structural evolution of the Basin and Range province. *Journal of Geophysical Research*, *94*(B2), 1765–1775.

Suppe, J. (2014). Fluid overpressures and strength of the sedimentary upper crust. *Journal of Structural Geology*, *69*, 48–492.

Tesei, T., Collettini, C., Carpenter, B. M., Viti, C., & Marone, C. (2012). Frictional strength and healing behavior of phyllosilicate-rich faults. *Journal of Geophysical Research*, *117*, B09402. https://doi.org/10.1029/2012JB009204

Wernicke, B. (1981). Low-angle normal faults in the Basin and Range Province: Nappe tectonics in an extending orogen. *Nature*, *291*, 645–648.

Wernicke, B., & Axen, G. J. (1988). On the role of isostasy in the evolution of normal fault systems. *Geology*, *16*(9), 848–851.

Xiao, H.-B., Dahlen, F. A., & Suppe, J. (1991). Mechanics of extensional wedges. *Journal of Geophysical Research*, *96*(B6), 301–318.

Yuan, X. P., Christie-Blick, N., & Braun, J. (2018). *Mechanical properties of the Sevier Desert detachment* (Vol. 45, pp. 7417–7424). Geophysical Research Letters: An application of critical Coulomb wedge theory. https://doi.org/10.1029/2017GL076854

Yuan, X. P., Leroy, Y. M., & Maillot, B. (2015). Tectonic and gravity extensional collapses in overpressured cohesive and frictional wedges. *Journal of Geophysical Research: Solid Earth*, *120*, 1833–1854. https://doi.org/10.1002/2014JB011612